JMATPRO	Journal of Advanced Materials and Processing 13 (50): 3-18, 2025 https://sanad.iau.ir/journal/jmatpro Doi: 10.71670/jmatpro.2025.1194442

Research Paper

Numerical and Experimental Investigation of the Erosion Resistance of YSZ and GZ+YSZ Coatings on Inconel 738

Mohsen Rahnavard[1], Majid Jamal-Omidi[2*], Majid Tavakolian[1], Nader Mohammadi[3]

1. Department of Mechanical Engineering, WT.C., Islamic Azad University, Tehran, Iran
2. Faculty of Aerospace Engineering, Malek-Ashtar University of Technology, Tehran, Iran
3. Department of Mechanical Engineering, Pa.C., Islamic Azad University, Tehran, Iran

ARTICLE INFO

Article history:

Received 24 December 2024
Revised: 15 January 2025
Accepted 10 February 2025
Available online 21 April 2025

Keywords:
Coating
Erosion
Finite element
Inconel
Impact
YSZ
GZ+YSZ
Thermal barrier coating

ABSTRACT

In this study, the erosion resistance of YSZ and GZ+YSZ coatings on Inconel 738 under alumina particle impact was investigated both numerically and experimentally. In the experimental phase, the mass loss of the samples was measured from the initial to the final state under controlled laboratory conditions. The numerical analysis was performed using ABAQUS finite element software alongside a developed MATLAB code. This analysis examined various factors, including compressive stress, fracture energy, multiple particle impacts, particle velocity, impact angle, particle diameter, and the random spatial distribution of impacts. The total erosion and final mass loss were estimated, and the results were validated against the experimental data. The findings indicate that the erosion rate of the YSZ ceramic coating is lower than that of the GZ+YSZ coating, which experienced a mass loss 38% greater than that of the YSZ coating. The erosion rate for both coatings was observed to decrease initially before increasing over time. Furthermore, multiple impacts at the same location and particle size were found to have an insignificant effect on the erosion rate. Reducing the impact angle from normal (90°) and lowering particle velocity decreased the erosion rate. This research provides an analysis of the underlying causes for these observations and evaluates the dominant erosion mechanisms and coating behaviors.

Citation: Rahnavard, M.; Jamal-Omidi, M.; Tavakolian, M.; Mohammadi, N. (2025). Numerical and Experimental Investigation of the Erosion Resistance of YSZ and GZ+YSZ Coatings on Inconel 738, Journal of Advanced Materials and Processing, 13 (50), 3-18. Doi: 10.71670/jmatpro.2025.1194442

[*] **Corresponding Author:**
E-Mail: j_omidi@mut.ac.ir

1. Introduction

Thermal Barrier Coatings (TBCs) are typically applied to components that require high thermal endurance, such as gas turbine parts [1]. TBC materials are usually ceramics-based, offering a high coefficient of thermal expansion with low strain amounts, and are mostly used in parts exposed to high temperatures [2]. These coatings are often subjected to thermal effects, which have been investigated both experimentally and numerically [3–6].

Components in high-technology industries, such as aerospace and power generation, are often analyzed primarily with respect to thermal effects. However, erosion of thermal barrier coatings can also significantly affect their lifetime and performance [7]. It is worth mentioning that the erosion behavior of coatings plays a significant role in the decision-making process regarding the use of TBCs [8]. The study of static and dynamic conditions, along with the development process, moves the problem out of the state of monosyllabic investigation on coatings.

In simple terms, erosion refers to the collision of high-speed fine particles suspended in air, soil, soot, etc., with components or devices. Depending on the movement conditions of the mentioned particles, erosion causes corrosion and mass reduction of the parts. Erosion is one of the major challenges in various industries, leading to degraded characteristics and even damage or failure of components [9]. Consequently, erosion is widely studied in many engineering investigations and various experimental tests [8,10,11].

The erosion of componentsis influenced by parameters such as particle velocity, impact angle, material properties of the eroded surface, etc. [9]. Due to the complex nature of the impactor, investigating these conditions involves significant complexity [12]. Simply put, impact can be described as a dynamic vibrational state of the structure under very high frequencies over a short duration [13]. This complexity becomes more pronounced when the eroded part undergoes permanent damage or mass loss [14]. Since conducting various experimental tests to understand erosion is time-consuming and costly, numerical modeling of TBC coatings greatly assists in comprehending these phenomena.

As reported by Gee and Hutchings, material erosion can be classified into ductile and brittle regimes [9]. It is also explained that the particle velocity, size, and impact angle significantly influence the extent and rate of erosion [15]. The effect of velocity on the erosion of titanium has been experimentally studied by Yan et al. [16,17].

With advances in numerical methods, recent studies have increasingly employed computational approaches to investigate erosion. For instance, Liu et al. conducted a finite element analysis on the influence of particle shape on material erosion [18]. Zhao et al. examined the surface morphology of eroding objects post-impact and performed statistical comparisons with experimental data [11]. Zheng et al. studied multiple impact parametersfrom several eroding particles at the same location [8]. Xiao et al. investigated strain rate effects in single-impact collisions using a similar approach [19]. Furthermore, the same methodology was applied to analyze the effects of crude oil on the erosion rates of steels 1044 and J55 [20]. Additional studies have explored factors such as surface modeling [11], the type of surface curvature [21], thermal shock effects on erosion rate [22], and the influence of fluid and mass flow on erosion [23].

The study of erosion behavior is not limited to impact and contact modeling; in some cases, computational fluid dynamics (CFD) can also be employed. Many studies, including those by Mansouri et al. [24], have combined experimental and numerical results using CFD methods [25–28]. In such modeling, erosion behavior is predicted by simultaneously solving the molecular and structural dynamics. However, since most erosion investigations focus on structural dynamics, detailed fluid analyses are often omitted.

To reduce computational time and simplify problem analysis, most studies employ symmetric or semi-symmetric approaches in numerical modeling. It is worth noting that some numerical investigations on the erosion behavior of YSZ and GZ TBC coatings have also been reported. However, most existing research is based on experimental or semi-numerical methods and examines coating erosion statistically [29].

In the present study, numerical methods are used to investigate the erosion behaviors of YSZ and GZ coatings on Inconel 738 under alumina particle impact. Experimental test results were utilized to develop the numerical model, which was implemented in ABAQUS commercial software to simulate the erosion process. For simplicity and clearer visualization, the problem was solved using a quasi-two-dimensional symmetric approach. This allows the results to be effectively evaluated and compared with microscopic experimental images. Following the numerical solution phase, a parametric study on the TBC coating erosion was conducted. This study examines the influence of parameters such as particle diameter, velocity, compressive yield stress, G_{IC} (fracture energy), impact angle, and the effect of multiple particles impacting the same location. Erosion resulting from multiple particle impacts at a single site constitutes the subsequent

phase of investigation. A MATLAB code was developed for this purpose, enabling the estimation of total erosion by combining parametric study results with random impact simulations. Finally, these results were compared with the experimental data. The overall workflow is illustrated in Fig. 1. The comprehensive investigation of YSZ, GZ, and their combination thermal barrier coatings through integrated experimental and numerical methods constitutes the novelty of the present study.

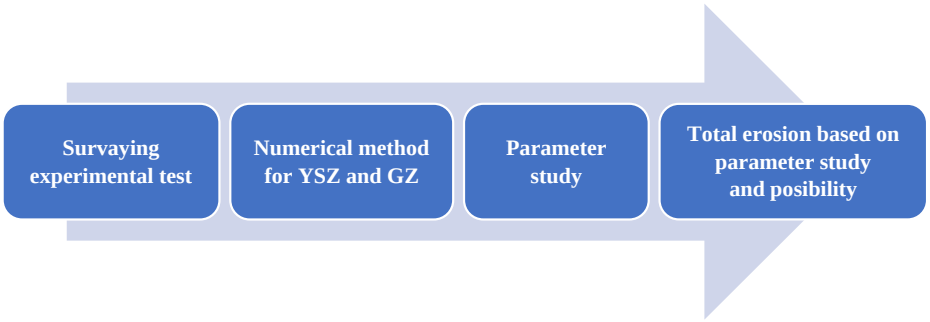

Fig. 1. Research workflow.

2. Experimental erosion tests

2.1. Materials

The experimental tests serve as the basis for validating the numerical study. The substrate material used in the tests is Inconel 738, with a mean chemical composition of Ni-8.5Co–16Cr–3.4Al–3.4Ti–2.6W–1.7Ta–1.7Mo–0.9Nb–0.1C (wt-%). The top coatings consist of YSZ and GZ layers, either separately or in combination. The bond coat material is Amdry® 962-NiCrAlY. For the top coat, Metco® 204NS-G-YSZ Zirconia powders and Ottochemi® G 2007 GZ powder were used.

2.2. Air plasma spraying (APS)

To enhance surface roughness and coating adhesion, the substrates were grit-blasted using 25-grain-mesh SiC particles before plasma spraying. The specimens were then cleaned and degreased with absolute acetone in an ultrasonic bath and preheated at 150-200 °C. APS was performed using a Metco® 3MB system. The primary and secondary plasma gases were argon and hydrogen, respectively. The spraying parameters for each coating are summarized in Table 1.

Table 1. Plasma spraying parameters for each coating.

Parameter	NiCrAlY	YSZ	GZ
Current (A)	500	550	500
Voltage (V)	80	70	70
Primary gas flow, Ar (l/min)	85	85	85
Secondary gas flow, H2 (l/min)	15	15	15
Powder feed rate (g/min)	42	37	37
Spray distance (mm)	130	120	80
Wheel rotation speed (rpm)	35	25	35

A NiCrAlY bond coat with a thickness of 150 µm was first deposited via plasma spraying onto the specimens. The primary coated specimens were then plasma sprayed with the two following coatings:

1. Normal YSZ with a thickness of 300 µm.
2. Composite layer consisting of 50 µm YSZ over the bond coat, followed by 250 µm GZ.

2.3. Erosion test

Erosion tests were performed according to ASTM G76-13 at room temperature using a high-pressure gas gun erosion rig. Alumina particles with a nominal size of 300 µm were impacted at 90° (normal incidence), as illustrated in Fig. 2. The gun was positioned 10 mm from the sample surface and operated at a pressure of 5.52 bar. Each coating sample was subjected to 12 repeated erosion tests. Each test lasted 10 minutes, with the weight loss of the sample measured at 2-minute intervals.

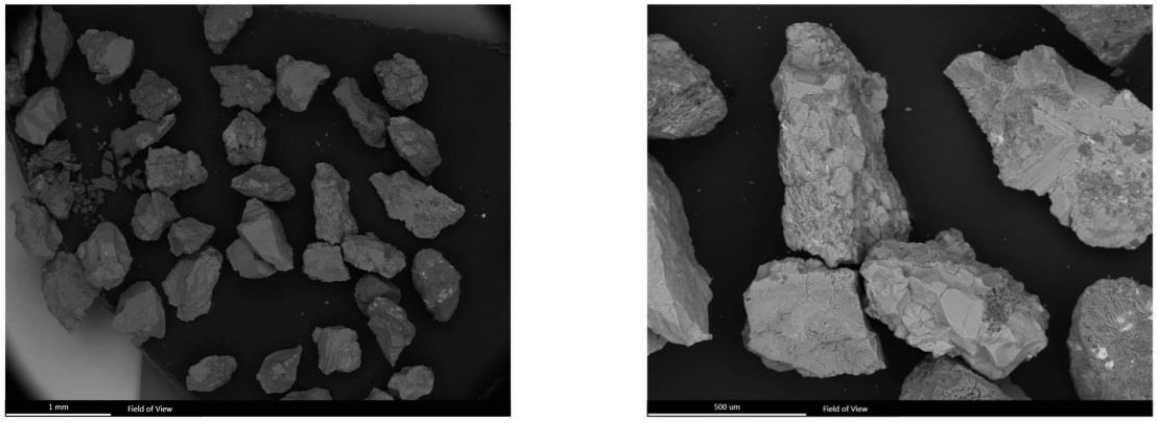

Fig. 2. SEM images of alumina objects.

Based on the semi-empirical Eq. 1, the collision velocity of the alumina particles was calculated [9].

$$V^2 = \frac{kP}{d^{0.57}\rho^{1.08}} \quad (1)$$

where P is the mass flow pressure (kPa), d is the erosion particle size (μm), and ρ is the particle density (kg/m^3). The constant k is taken as 7900. Assuming a particle size of 300 μm and an alumina density between 3000 and 4000 kg/m^3, the collision velocityis approximately 30 m/s.

2.4.Erosion test results

During the tests, the particle flow rate during impacts ranged from 0.03 to 0.05 g/s. Each erosion lasted 10 minutes; therefore, 15 to 20 grams of alumina particles eroded the relevant surfaces, which is consistent with the experimental conditions reported in reference [10].

The mean weight loss of specimens during the erosion tests is presented in Table 2 and illustrated in Fig. 3. Table 2 also lists the mean weight losses for each sample over 12 repeated tests along with the corresponding standard deviation values.

Table 2. Mean weight loss of coating samples during erosion tests.

Erosion Time (min)		2	4	6	8	10	Total
YSZ	Mean sample weight loss (mg)	10.04	5.633	3.508	5.133	3.192	27.50
	Standard deviation	3.92	1.322	1.558	1.493	0.788	3.80
YSZ/GZ	Mean sample weight loss (mg)	12.03	12.480	3.308	5.333	4.675	37.826
	Standard deviation	3.84	3.670	1.602	1.318	2.324	6.27

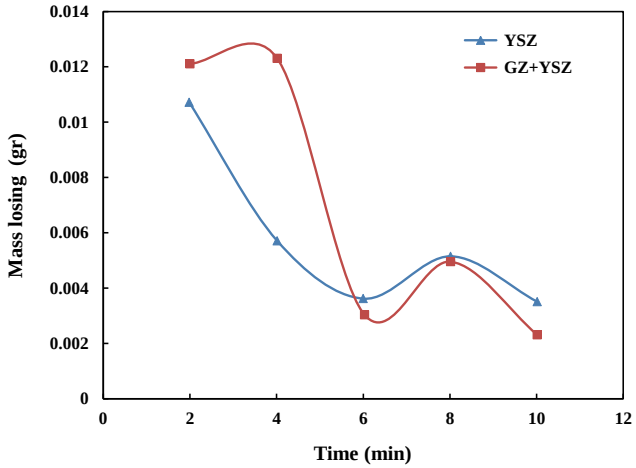

Fig. 3. Mass loss of the two coatings.

Based on the results in Table 2, after the 10-minute erosion test, the usual YSZ TBC exhibits significantly higher erosion resistance compared to the GZ-containing sample. Similar studies have reported that due to the lower toughness of GZ relative to YSZ, GZ coatings possess considerably poorer erosion resistance than YSZ TBCs [10]. The high fracture energy of YSZ compared to the GZ

highlights the importance of accurately accounting for fracture effects and their representation in numerical modeling. Furthermore, an important observation from the curve is that the erosion rate in both coatings initially decreases over time and then increases. This trend can be attributed to the increase in surface roughness during collision time. As roughness increases, the effective impact angle deviates from the normal 90°, leading to a reduction in erosion rate–a finding consistent with results reported in the reference [9]. This phenomenon, along with related parametric studies, will be further discussed in the numerical analysis section.

As indicated in Table 2, the average mass loss of the YSZ coating is 27.5 mg, whereas that of the GZ+YSZ coating is approximately 37.8 mg. This corresponds to an approximately 38% greater mass loss in the GZ+YSZ coating compared to the YSZ coating.

3. Numerical modeling

The dynamic explicit finite element method implemented in ABAQUS was employed to simulate the erosion process. To enhance computational efficiency and simplify result interpretation, the problem was modeled using a two-dimensional symmetric approach. In accordance with the experimental setup, both YSZ and YSZ+GZ coatings were investigated separately. Spherical alumina erodent particles with radius ranging from approximately 150 to 200 μm were modeled as rigid bodies, corresponding to the experimental conditions. Since TBC coating are the first materials subjected to impact, the ceramic layers were finely meshed. In the impact zone and its vicinity, an element size of 1 μm was used, while the outer regions were assigned a coarser mesh of 50 μm. The Inconel substrate, which is affected only in later stages, was discretized with a coarse mesh to reduce computational cost.

Mesh convergence was ensured through a sensitivity study. Due to the critical interface between the coating and the Inconel base, a refined mesh was adopted in that region. The initial mesh density was set to 10 elements along both the radial and height directions, and progressively increased up to 100 elements. Most of the concentration of the number of elements was at the impact location, such that it increased at a rate of 1.1 from the center of the radius and height. The number of elements was initially 2000 and continued to 12500, and by examining the removal of elements due to damage and the stability of the images, this mesh convergent validation was performed. An example of the finite element model for YSZ and GZ+YSZ coatings along with the alumina material is illustrated in Fig. 4.

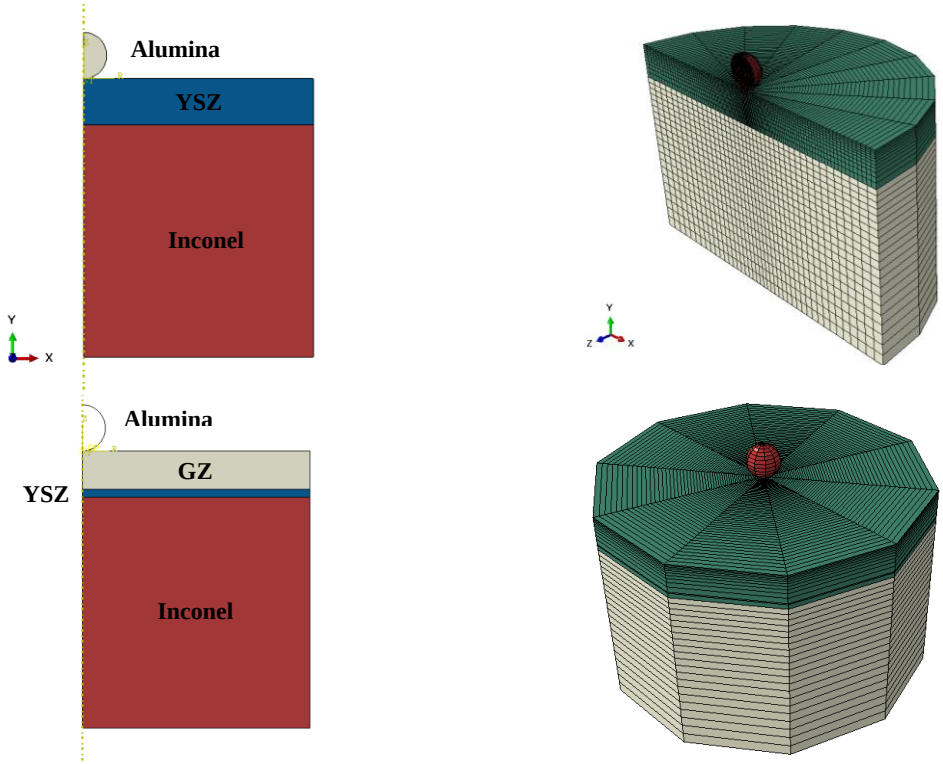

Fig. 4. Finite element modeling of two TBCs: YSZ and GZ+YSZ.

The model is constructed in two-dimensional ax-symmetric form; a full rotation of the profile generates a cylindrical geometry. The lower boundary of the model is fixed. The particle is modeled as a rigid body, so no elements are removed from it during the impact, and most of the energy is

transferred into the coating model for damage analysis. A contact formulation is defined between the particle and the coating, and the meshing is configured such that damage can be captured across all elements of the coating model.

4. Mechanical behavior, damage, and fracture

The mechanical properties of the materials used are important and must be accurately represented under the simulated conditions. A series of constitutive models is required to describe the mechanical behavior and properties, including elastic-plastic response, damage initiation, damage evolution, and equation of state. The damage process induced by impact during the tests is outlined schematically in Fig. 5.

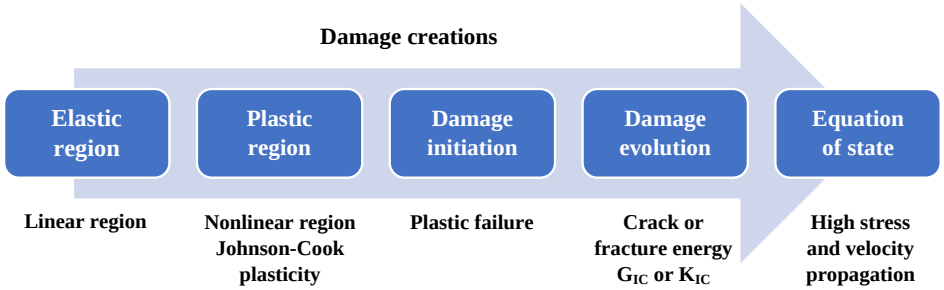

Fig. 5. Damage process during impact.

The elastic behavior is described by a linear elastic model defined by Young's modulus and Poisson's ratio. The plastic behavior of these materials is slightly different. The YSZ and GZ coatings are almost brittle, being ceramic materials, and tend to fail under low strain and stress. In contrast, Inconel 738 exhibits significant plastic deformation. The mechanical properties of ductile materials are represented by various constitutive models, which vary depending on the applied stress state. Among these, the Johnson-Cook plasticity model pointed out that depending on the type of triaxial stress or the ratio of total compressive stress to Von Mises stress, the behavior of plastic strain is different. The ceramic materials in the tensile state have much lower ultimate yield stress than in the compressive state, and this should be taken into account in the numerical analysis. Also, tensile and compressive failure behaviors should be considered different according to stress triaxiality, depending on the type of tensile and compressive stress.

Various models exist to describe damage initiation in the plastic regime. Among these, the Johnson-Cook dynamic failure model is well-suited for ductile materials. However, it is not comprehensive for brittle ceramic materials such as YSZ and GZ coatings. For such ceramics, damage initiation is better characterized by incorporating stress triaxially and strain rate effects, which will be further detailed in the mechanical properties section. Regarding damage evolution, the fracture energy and material properties of YSZ and GZ ceramic coatings influence their resistance to crack propagation and failure. An appropriate relation for describing damage evolution is given below [8]:

$$D = 1 - exp\left(-\int_0^{u^{pl}} \frac{\sigma_y u^{\cdot pl}}{G_f}\right) \tag{2}$$

where G_f is the fracture energy per unit of newly formed fracture surface, (J/m^2) and σ_y is the yield stress.

As noted, impact involves rapid transfer of stress and energy through the material. To capture the high-pressure, large-deformation response under such conditions, a suitable equation of state (EOS) is required. Various EOS formulations exist, among which the Mie-Grüneisen equation is widely used; its application requires specific material parameters [8]. In the present study, however, because the particle velocity remains below 100 m/s, such high-pressure state modeling is omitted. Consequently, two finite element techniques are employed to simulate erosion in the coatings:

1. Brittle-failure approach: Given the brittle nature of the ceramic coatings, plastic behavior is not defined. Instead, a yield stress is specified, at which point material failure is assumed to occur immediately.
2. Elemeny-deletion approach: Upon reaching the defined yield stress, elements are progressively removed from the simulation. In this method, yield stress marks the onset of damage, and once the fracture toughness is exceeded, the remaining impact

energy leads to complete element failure and removal.

4.1. Mechanical properties

The materials properties used in the numerical simulation are listed in Table 3. The values presented are based on a statistical review of various sources [9,30] and the CES Material Bank software, selecting the most representative data for the given conditions. For example, alumina properties vary with particle grade (e.g., 88, 90, 94); the values corresponding to the particle size used in the erosion tests were adopted. Similarly, the mechanical properties of YSZ depend on the Y_2O_3 content, which typically ranges from 0 to 10 wt% [30]. In this simulation, an 8% Y_2O_3 composition –consistent with the experimental material– was used.

Table3. Mechanical properties of materials used in the numerical simulation, based on references [9,30] and CES software.

Properties	YSZ	GZ	Inconel 738	Alumina
ρ (kg/m^3)	6000	6000	8110	3500
E (GPa)	180	200	203	275
ν	0.29	0.29	0.3	0.3
σ_y (MPa)	200	180	900	191
σ_{uT} (MPa)	200	180	1080	191
σ_{uC} (MPa)	600–6500	400–2900	–	2500
ε_u (%)	0.2	0.15	7	0.07–0.09
G_{IC} (J/m^2)	37.4 ± 10.1	5.8 ± 1.2	–	–
Vickers hardness	791 ± 150	92 ± 554	–	–

According to Table 3, the damage response of the coatings differs under tensile and compressive loading. Stress triaxially is used to characterize the stress state, where the ratio of mean stress to equivalent stress influences failure behavior in tension, compression, and shear. Stress triaxially ranges from -2/3 for biaxial compression to 2/3 biaxial tensile, with a value of zero corresponding to pure shear. Since ceramic coatings exhibit distinct tensile and compressive strengths, their failure behaviors under these stress states are modeled separately. Based on the fracture energy values listed in the table, the material model must capture crack initiation and propagation after yielding. Accordingly, the fracture energy (or critical energy release rate G_{IC}) is specified as given in the table. A parametric study incorporating both fracture energy and ultimate compressive stress is conducted to evaluate their influence. Boundary conditions are applied in the explicit dynamic simulation: the lower surface of the Inconel substrate is fully fixed in the thickness direction. A Tie constraint connects the YSZ or GZ coating to the substrate, allowing independent meshing of each layer. A solid spherical alumina particle is then impacted onto the coating surface at 30 m/s. The particle is constrained against rotation and lateral motion to ensure normal impact.

5. Numerical results

Given that the material undergoes damage evolution during impact, its properties must be degraded or removed; here, element deletion is employed. Because the TBC coating surface is particularly susceptible to such damage, contact between the alumina particle and the YSZ coating is modeled via element-based contact, as illustrated in Fig. 6 for different simulation stages.

To verify that the impactor fully engages with the sample surface and its velocity reduces to zero or changes sign, the velocity-time history is plotted in Fig. 7.

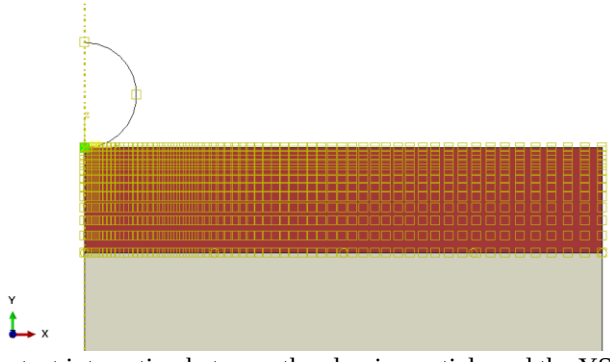

Fig. 6. Contact interaction between the aluminaparticle and the YSZ coating.

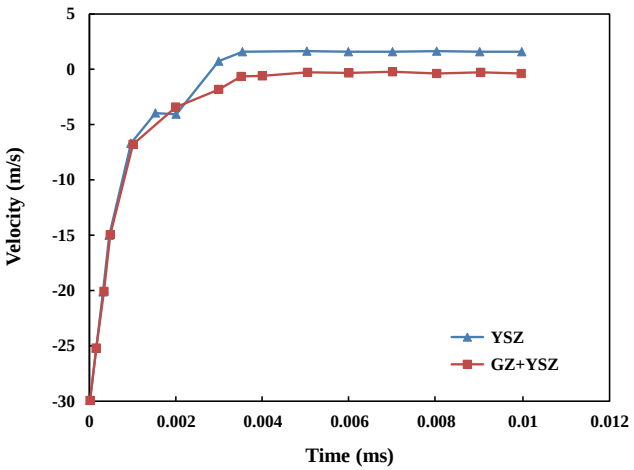

Fig. 7. Velocity of the alumina particleversus time for two coatings.

According to Fig. 7, when the alumina particleimpacts the YSZ coating surface, itsvelocity drops to zero within the first 20% of the contact duration. Subsequently, the particle reverses direction and moves away from the surface with a rebound velocity of approximately 1.4 m/s. In contrast, for the GZ-containing coating, the velocity does not reverse and instead approaches nearly zero. This difference in rebound behavior is attributed to the higher fracture energy of YSZ compared to GZ, which allows more elastic energy to be returned to the particle, leading to its rebound. The erosion patterns of the two coatings after impact are shown in Fig. 8.

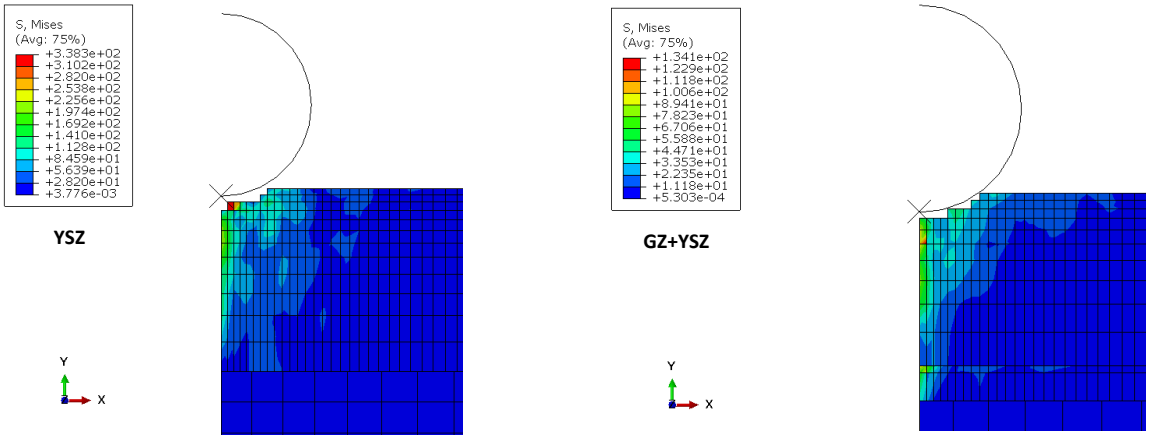

Fig. 8. Erosion results of the YSZ and GZ+YSZ coatings.

The minimum ultimate compressive stress was assumed for both TBC materials. Fracture energy values for damage evolution stages were taken from Table 3.

A key output of erosion analysis is the erosion rate [8,10,11], defined as the removed volume (or mass) per unit volume (or mass) of the eroded material. Since the density of the erodent differs from that of the coating, the volumetric erosion rate is used. To compute the volume loss during erosion, a Python script linked to ABAQUS was developed, which calculates the lost volume relative to the initial state. The erosion rate is then obtained by dividing this volume by the total volume (or mass) of impacting material.

Therefore, the calculated erosion rates for the YSZ coating is 4.91×10^{-4} mm^3/mm^3, while the rate for the GZ coating is 6.08×10^{-4} mm^3/mm^3. This difference may be influenced by the visible element deletion in the simulations. The lower erosion rate of YSZ is attributed to its higher fracture energy and Vickers hardness compared to GZ.

To validate these results, the numerical erosion rates are compared with experimental data using the following relationship:

$$err = \frac{m_e}{n_z m_z}\frac{\rho_z}{\rho_e}\left(\frac{mm^3}{mm^3}\right) \quad (3)$$

In this relationship, m_e is the final eroded mass of the material, n_z and m_z are the total number and the approximate mass of each alumina particle, ρ_e and ρ_z are the density of the particle and the TBC coatings.
The particle mass is derived from its diameter and density. The number of particles is estimated from the gas flow rate used in the experimental tests. Based on this, the erosion rate for YSZ ranges between 5.0×10^{-4} and 9.0×10^{-4} mm^3/mm^3, while for GZ it ranges from 8.33×10^{-4} to 1.39×10^{-3} mm^3/mm^3, indicating a comparable order of magnitude for both materials.
Besides the higher erosion rate of GZ, the stress transferred to the underlying layers –particularly the Inconel substrate– is more pronounced in YSZ than in the GZ+YSZ system, as illustrated in Fig. 9. This figure presents the Von Mises stress history at the substrate-coating interface for both coating types.

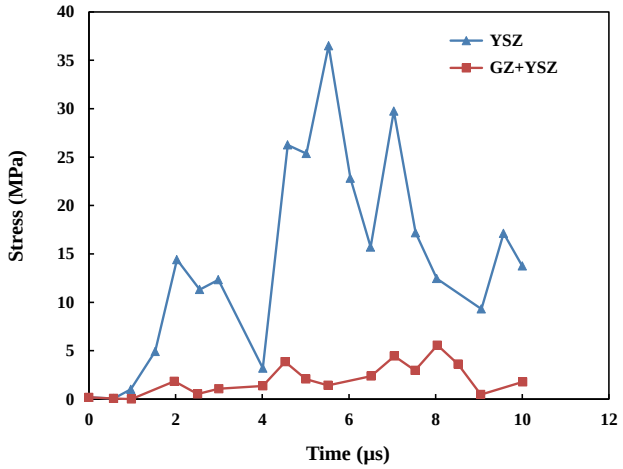

Fig. 9. Stress versus time at the substrate/coatings interfaces of two TBC systems.

Thus, the combined GZ+YSZ coating exhibits a higher erosion rate than YSZ alone. Its bilayer structure also reduces the stress transmitted to the underlying substrate. Consequently, the Von Mises stress reaching the Inconel substrate is reduced by approximately one-tenth in the GZ+YSZ system compared to the YSZ coating alone.
To illustrate the temporal distribution of impact force, Fig. 10 presents the force-time history for both coatings. This diagram also complements the velocity-time curve (Fig. 7) in understanding the particle-surface interaction. As shown in Fig. 10, the contact force exerted by the alumina particle on the YSZ coating is significantly lower than that on the GZ coating, which contributes to the lower erosion rate of YSZ. A notable feature of the force-time curves is the oscillatory force response during impact in both coatings. The force initially rises, then approaches zero, rises again, and finally decays to zero as the energy is fully dissipated. This behavior can be attributed to the brittle nature of the ceramic TBCs: upon impact, fragments are ejected and may re-impact the surface, transferring residual energy in discrete stages.

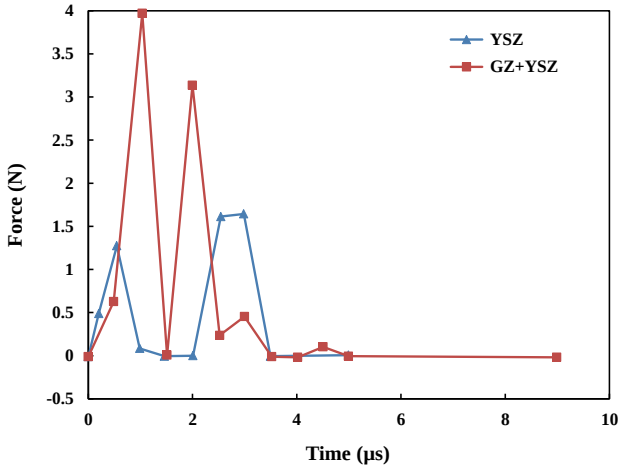

Fig. 10. Impact force versus time for the alumina particle.

6. Parametric study

The previous section described the fundamentals of the erosion test. Here, a parametric study is conducted to determine the overall erosion rate resulting from the random impact of tens of thousands of particles on the TBC coatings. The effects of the following parameters on the erosion rate are examined: compressive yield stress, fracture energy, multiple particle impact on surfaces, particle velocity, impact angle, and particle diameter. The resulting erosion rate trends are presented as functions of these parameters.

6.1. Effect of compressive strength and fracture energy

As noted, the compressive strength of ceramic coating is considerably higher than its tensile strength, which correlates with Vickers hardness. In experimental tests, compressive strength ranges from 500 to 6500 MPa, depending on the manufacturing process. Erosion test results indicate that variations in compressive stress have a negligible influence on the erosion rate.

Fracture energy for such materials typically lies between 0 and 40 J/m^2. Numerical simulations show that the erosion rate decreases as fracture energy increases. To examine this in detail, Fig. 11 displays the stress contour at the moment of impact for two fracture energy values: 0 and 40 J/m^2.

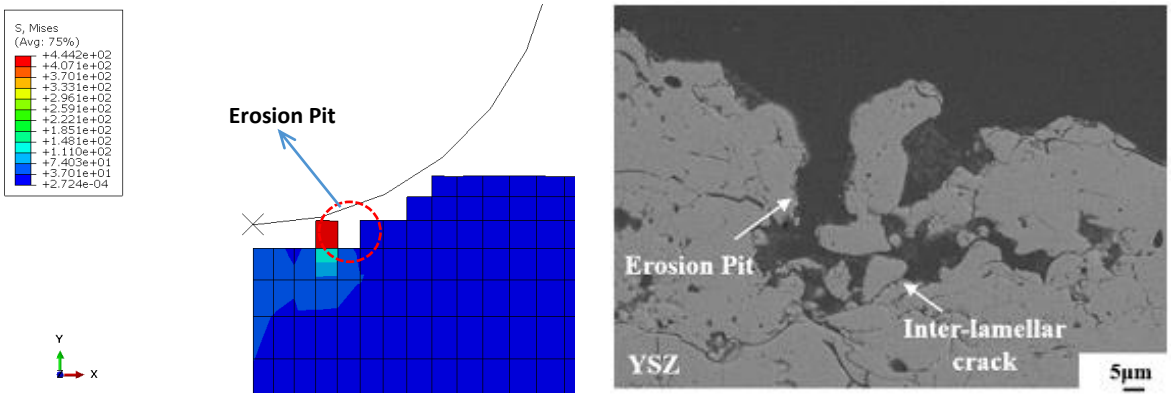

Fig. 11. Stress contour under erosion for material with zero fracture energy, compared with available experimental result.

The results indicate that under zero fracture energy – representing a more brittle state– failure leads to hole formation during loading. The ceramic coating appears to exhibit much lower fracture energy in the simulation than observed experimentally, a critical factor to consider in decision-making processes. The variation of erosion rate with compressive yield stress and fracture energy for both coatings is presented in Fig. 12. As shown, the erosion rate decreases with increasing fracture energy and becomes negligible beyond a certain threshold.

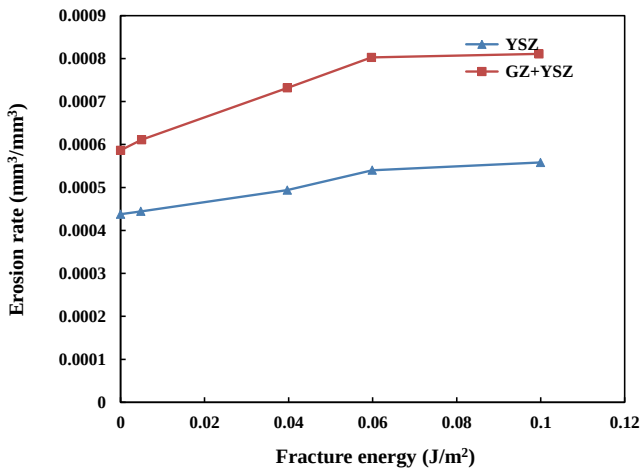

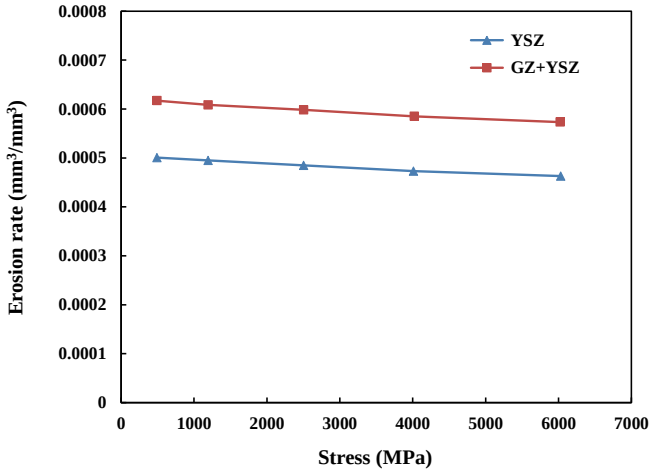

Fig. 12. Erosion rate as a function of fracture energy and compressive strength.

6.2. Multiple particle impact at a single location

To study the effect of multiple impacts at the same site, three particles were sequentially impacted at specified intervals, as illustrated in Fig. 13, and the resulting erosion rate was computed. The calculation shows that consecutive impacts at the same location do not significantly alter the erosion rate.

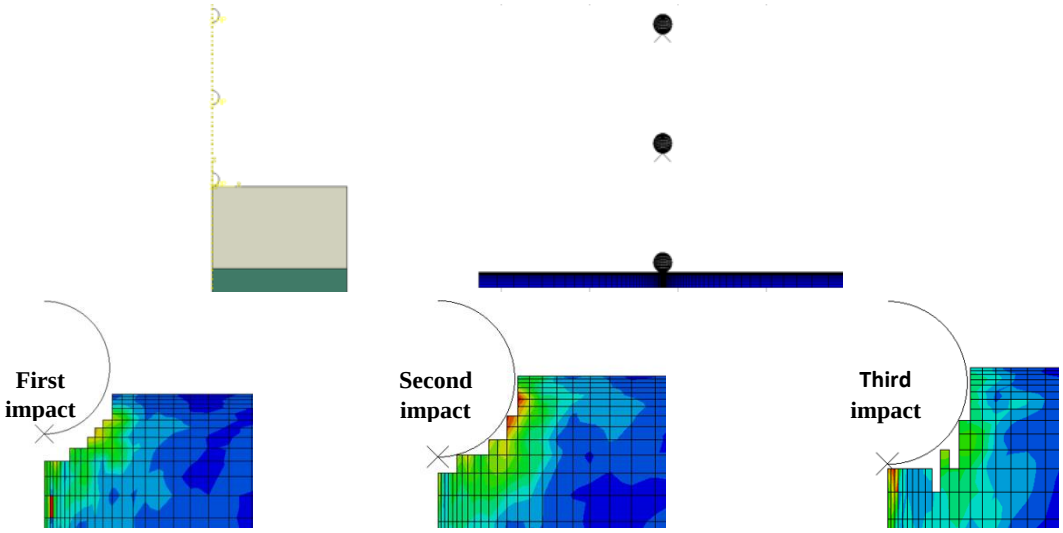

Fig. 13. Modeling erosion under successive impactsat a single location.

6.3. Effect of impact angle

In the TBC erosion tests, particles impact at approximately 90° (normal incidence). However, as erosion progresses, material removal increases surface roughness, which effectively alters the local impact angle. To account for this, numerical simulations were performed at various impact angles. The alumina particle velocity was resolved into x- and y-components according to the desired angle, and the resulting erosion patterns are shown in Fig. 14. As observed, the erosion rate gradually decreases as the impact angle is reduced, a trend consistent with findings reported in the references [9].

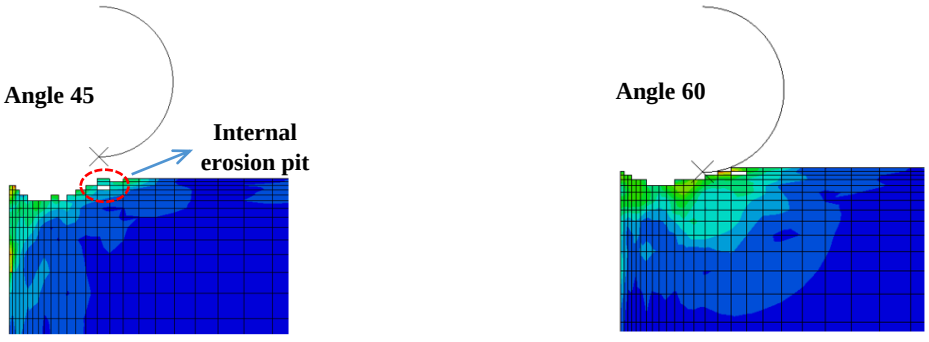

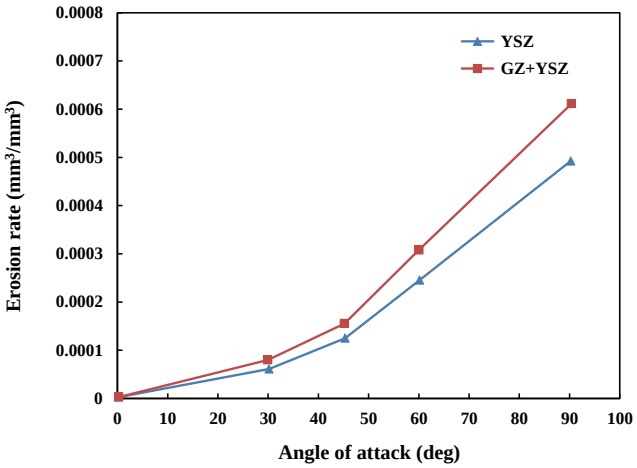

Fig. 14. Erosion rate under oblique particle impact.

6.4. Effect of particle velocity and size

Particle velocity and size significantly influence erosion due to their direct effect on kinetic energy. According to prior study [9], velocity is the primary factor enhancing erosion, with the erosion rate typically proportional to velocity raised to a power between 14.2 and 25. However, another investigation [10] suggests that beyond a certain velocity range, further increases do not raise the erosion rate, a behavior that can be explained by the equation of state [8]. Under the experimental conditions used here, the effect of particle velocity and size on the erosion of YSZ and GZ+YSZ coatings was examined at a nominal velocity of 30 m/s and a particle diameter of 150 µm. In the parametric study, the particle diameter was varied from 50 to 800 µm, accounting for changes in particle mass. The results show that the erosion rate remains relatively unchanged across this size range, as the increase in particle mass and volume counterbalances other influencing factors –a trend also noted in reference [9]. The influence of velocity follows a different pattern. At relatively low velocities (below ~100 m/s), where the equation of state has limited effect, the erosion rate varies considerably with changes in velocity. This dependence is evident in the stress contours and plots presented in Fig. 15.

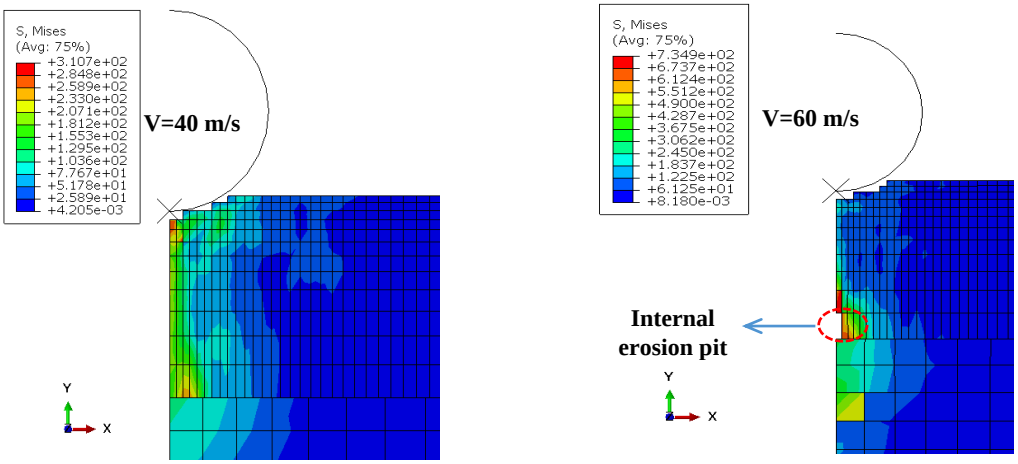

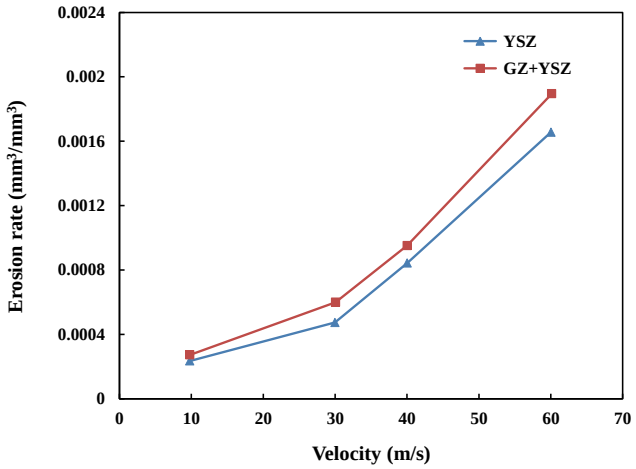

Fig. 15. Erosion rate variation with particle velosity.

It is concluded that the erosion rate is strongly velocity-dependent, scaling approximately with the square of velocity. Mass loss in the model is primarily associated with crack propagation, especially near the interface between the Inconel substrate and the TBC. This failure mode is referred to as inter-layer cracking.

6.5. Estimation of total erosion rate

To comprehensively assess erosion and its governing parameters, a flat erosion surface was generated in MATLAB. Particles were then impacted onto this surface in a fully random manner with an average velocity of 30 m/s. The impact conditions and erosion rates were assigned based on the parametric study results, accounting for factors such as impact angle. The overall surface erosion was computed and visualized. In this step, the sample surface subjected to erosion was assumed to have rectangular dimensions of 30 mm ×30 mm × 2 mm, consistent with the experimental setup. Over time, the erosion rate was calculated considering probable impacts, and the results for the YSZ coating are presented in Fig. 16.

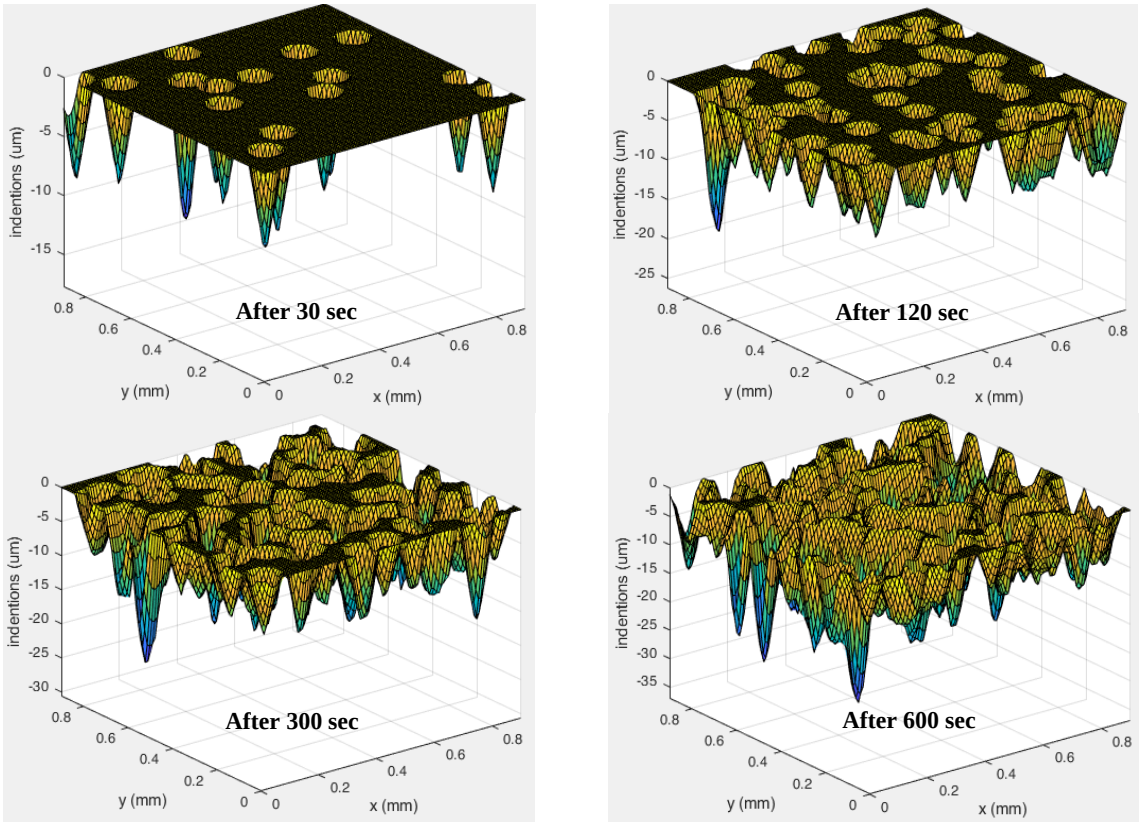

Fig. 16. Evolution of surface contour for the YSZ coating in terms of time.

In the contour plot of the 30 mm rectangular section (Fig. 16), only results within a 1 mm depth limit are displayed. The time-dependent contour changes of the eroded surface reflect the outcomes of the numerical-statistical analysis of random particle impacts during the erosion test. Finally, the temporal variation of mass loss for both YSZ and GZ+YSZ coatings is presented in Fig. 17.

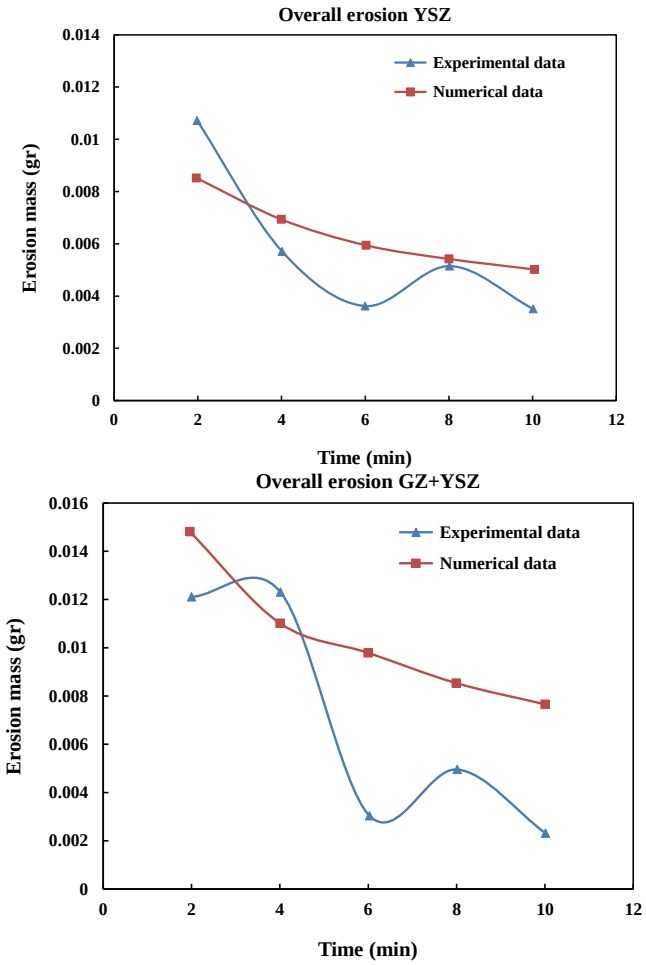

Fig. 17. Comparison of overall erosion rate with experimental data.

Based on the overall erosion rate obtained from probabilistic impact simulations, the mass loss for the YSZ coating is approximately 30 g numerically and 27.5 g experimentally, showing good agreement. The erosion contour also reveals that the highest erosion occurs during the initial ~30 seconds, when the TBC surface is still relatively flat. Over time, the erosion rate decreases as the surface roughens, but then increases again due to repeated impacts –a trend observed in both numerical and experimental results.

7. Conclusion

This study developed a numerical model to simulate erosion in TBCs. Two coating systems –YSZ and GZ+YSZ– were investigated and compared with experimental data. The following are the main conclusions:

- The single-layer YSZ coating exhibits lower mass loss than the GZ-containing coating.
- The high fracture energy and Vickers hardness of YSZ contribute to its lower erosion rate compared to GZ.
- The double-layer GZ+YSZ coating transmits less stress and vibration to the underlying Inconel substrate.
- Variations in compressive yield stress have minimal influence on erosion rate, whereas fracture energy directly affects it.
- Multiple impacts at the same location do not significantly alter the erosion rate.
- The angle of impact from vertical to horizontal reduces the erosion rate to zero, mainly due to the material's brittleness.
- Increasing particle velocity raises the erosion rate exponentially within the studied range.
- Particle diameter has a negligible effect on erosion rate over the range examined (50-800 μm)

8. References

[1] N.P. Padture, M. Gell, E.H. Jordan, Thermal barrier coatings for gas-turbine engine applications, Science296(5566) (2002) 280-284.
[2] V. Kumar, K. Balasubramanian, Progress update on failure mechanisms of advanced thermal barrier coatings: A review, Progress in Organic Coatings 90 (2016) 54-82.
[3] M. Rahnavard, M. Ostad Ahmad Ghorabi, M. Rahnein, H. Rafiee, Effects of incorporation of micro and nano Al_2O_3 layers on thermal shock behaviour of YSZ thermal barrier coatings, Canadian Metallurgical Quarterly55(3) (2016) 312-320.
[4] M. Ranjbar-Far, J. Absi, S. Shahidi, G. Mariaux, Impact of the non-homogenous temperature distribution and the coatings process modeling on the thermal barrier coatings system, Materials & design32(2) (2011) 728-735.
[5] X. Zhang, M. Watanabe, S. Kuroda, Effects of residual stress on the mechanical properties of plasma-sprayed thermal barrier coatings, Engineering Fracture Mechanics110 (2013) 314-327.
[6] S. Widjaja, A.M.Limarga, T.H. Yip, Modeling of residual stresses in a plasma-sprayed zirconia/alumina functionally graded-thermal barrier coating, Thin Solid Films434(1-2) (2003) 216-227.
[7] J.H.Griffin, A review of friction damping of turbine blade vibration, International Journal of Turbo and Jet Engines7(3-4) (1990) 297-307.
[8] C. Zheng, Y. Liu, C. Chen, J. Qin, S. Zhang, Finite element analysis on the dynamic erosion process using multiple-particle impact model, Powder Technology 315 (2017) 163-170.
[9] M.G.Gee, I.M. Hutchings, General approach and procedures for erosive wear testing, Measurement Good Practice Guide No. 56. Reproduced by permission of the Controller of HMSO, ISSN 1368-6550, National Physical Laboratory Teddington, Middlesex, United Kingdom, TW11 0LW, 2002.
[10] D. Gonçalves, I. Sánchez-Arce, L. Ramalho, R. Campilho, J. Belinha, A meshless crack propagation algorithm extended to mixed-mode loading of adhesive joints, Composite Structures 305 (2023) 116502.
[11] X. Zhao, G. Tang, Z. Liu, Y.W. Zhang, Finite element analysis of anti-erosion characteristics of material with patterned surface impacted by particles, Powder Technology 342 (2019) 193-203.
[12] H. Liu, Z. Zhou, M. Liu, A probability model of predicting the sand erosion profile in elbows for gas flow, Wear 342 (2015) 377-390.
[13] G. Szuladzinski, Formulas for mechanical and structural shock and impact, CRC Press, 2009.
[14] M. Jafari, Z. Mansoori, M.S.Avval, G.Ahmadi, A.Ebadi, Modeling and numerical investigation of erosion rate for turbulent two-phase gas-solid flow in horizontal pipes, Powder Technology267 (2014) 362-370.
[15] Y.I.Oka, K. Okamura, T. Yoshida, Practical estimation of erosion damage caused by solid particle impact: Part 1: Effects of impact parameters on a predictive equation, Wear 259(1-6) (2005) 95-101.
[16] C. Yan, W. Chen, Z. Zhao, Experimental study on the high-speed impact of a sand particle on Ti-6Al-4V, Proceedings of the Institution of Mechanical Engineers, Part J234(4) (2020) 632-646.
[17] C. Yan, W. Chen, Z. Zhao, L. Liu, A probability prediction model of erosion rate for Ti-6Al-4V on high-speed sand erosion, Powder Technology364 (2020) 373-381.
[18] Z.G.Liu, S.Wan, V.Nguyen, Y. Zhang, A numerical study on the effect of particle shape on the erosion of ductile materials, Wear 313(1-2) (2014) 135-142.
[19] L. Xiao, X. Xu, H. Wang, A comparative study of finite element analysis of single-particle impact on mild steel with and without strain rate considered, International Journal of Impact Engineering 159 (2022) 104029.
[20] P. Wongpanya, Y. Saramas, C. Chumkratoke, A. Wannakomol, Erosion-corrosion behaviors of 1045 and J55 steels in crude oil. Journal of Petroleum Science and Engineering189 (2020) 106965.
[21] X. Zhao, G. Tang, Z. Liu, Y.W. Zhang, Numerical investigation of erosion characteristics of multiple-particle impact on ductile material with patterned surfaces, Powder Technology362 (2020) 527-538.
[22] M. Li, H. Ni, G. Wang, R. Wang, Simulation of thermal stress effects in submerged continuous water jets on the optimal standoff distance during rock breaking, Powder Technology 320 (2017) 445-456.
[23] R.J.Wood, A.D.Cook, Erosion-Corrosion in Pipe Flows of Particle-Laden Liquids, In Advances in Slurry Technology: IntechOpen, 2022.
[24] A. Mansouri, H. Arabnejad, S. Shirazi, B. McLaury, A combined CFD/experimental methodology for erosion prediction, Wear332 (2015) 1090-1097.
[25] G.V. Messa, Q. Yang, O.E. Adedeji, Z. Chára, C.A. Duarte, V. Matoušek, M.G. Rasteiro, R.S. Sanders, R.C. Silva, F.J. de Souza, Computational fluid dynamics modelling of liquid-solid slurry flows in pipelines: State-of-the-art and future perspectives, Processes9(9) (2021) 1566.
[26] S.K.Wee, Y.J.Yap, CFD study of sand erosion in pipeline, Journal of Petroleum Science and Engineering176 (2019) 269-278.
[27] R.E.Vieira, A. Mansouri, B.S.McLaury, S.A.Shirazi, Experimental and computational study of erosion in elbows due to sand particles in air flow, Powder Technology288 (2016) 339-353.
[28] J. Zhao, J. Ge, A. Khudoley, H. Chen, Numerical and experimental investigation on the material

removal profile during polishing of inner surfaces using an abrasive rotating jet, Tribology International 191 (2024) 109125.
[29] J. Alqallaf, N. Ali, J.A. Teixeira, A. Addali, Solid particle erosion behaviour and protective coatings for gas turbine compressor blades-A review, Processes8(8) (2020) 984.
[30] J. Kondoh, H. Shiota, K. Kawachi, T. Nakatani, Yttria concentration dependence of tensile strength in yttria-stabilized zirconia, Journal of alloys and compounds 365(1-2) (2004) 253-258.